PCCP

Accepted Manuscript

ROYAL SOCIETY OF CHEMISTRY

www.rsc.org/pccp

Strongly Bound Noncovalent $(SO_3)_n$:H_2CO Complexes (n = 1, 2)

Luis Miguel Azofra,[†] Ibon Alkorta[†] and Steve Scheiner[‡,] *

[†]Instituto de Química Médica, CSIC, Juan de la Cierva, 3, E-28006, Madrid, Spain

[‡]Department of Chemistry and Biochemistry, Utah State University, Logan, UT 84322-0300, USA

*Author to whom correspondence should be addressed.

Fax: (+1) 435-797-3390

E-mail: steve.scheiner@usu.edu

ABSTRACT

The potential energy surfaces (PES) for the SO_3:H_2CO and $(SO_3)_2$:H_2CO complexes were thoroughly examined at the MP2/aug-cc-pVDZ computational level. Heterodimers and trimers are held together primarily by S··O chalcogen bonds, supplemented by weaker CH··O or O··C bonds. The nature of the interactions is probed by a variety of means, including electrostatic potentials, AIM, NBO, energy decomposition, and electron density redistribution maps. The most stable dimer is strongly bound, with an interaction energy exceeding 10 kcal/mol. Trimers adopt the geometry of the most stable dimer, with an added SO_3 molecule situated so as to interact with both of the original molecules. The trimers are strongly bound, with total interaction energies of more than 20 kcal/mol. Most such trimers show positive cooperativity, with shorter S···O distances, and three-body interaction energies of nearly 3 kcal/mol.

KEYWORDS: chalcogen bond; CH··O H-bond; π-hole; cooperativity

INTRODUCTION

Noncovalent bonds,[1] such as hydrogen,[2-5] halogen,[6-11] pnicogen[12-20] or tetrel[21-24] interactions, act to hold together a wide range of dimers and larger aggregates. They are also essential ingredients in the structure adopted by many single molecules, as they can represent large fractions of the forces between segments that are not covalently bonded to one another. The chalcogen bond[25-35] is a closely related sort of noncovalent interaction which arises when a member of the chalcogen family (Y), e.g. O, S or Se, is drawn toward another electronegative atom (X), made possible in part by the anisotropic distribution of the electron density around Y. These Coulombic attractions are supplemented by charge transfer from the lone pair(s) of the X atom into the σ* or π* antibonding Z–Y orbitals (where Z is covalently bonded to Y), which tends to weaken and lengthen the latter Z–Y bond.[36-39]

Maxima and minima in the molecular electrostatic potential (MEP) represent plausible binding sites for interactions with partner molecules. Minima are typically associated with lone electron pair(s). Maxima can usually be classified into two main groups: i) σ-holes, which are localized along the extension of the Z–Y bond; and ii) π-holes, which are situated above the molecular plane.[37, 40-42] O_3, SO_2, SO_3 and SeO_2 are a few examples of small molecules that contain π-holes around the central chalcogen atom.[38, 39, 43] Understanding the behavior of these molecules when interacting with other substrates is a fundamental topic, due to their environmental and industrial importance.[44-48]

Our objective in the present work is a description of complexes containing SO_3 and H_2CO. Both are gases emitted into the atmosphere with severe environmental impact: SO_3 is the main compound involved in acid rain[44] and H_2CO is the major source of CO due to its photolytic decomposition in higher layers of the atmosphere.[49] Following a description of the electrostatic properties of the monomers, thorough examination of the entire potential energy surface (PES) of the SO_3:H_2CO heterodimer yields all minima. Careful scrutiny of these minima provides information on the strength and nature of the bonding that holds each together. A number of different minima are then located on the PES of the $(SO_3)_2$:H_2CO heterotrimer. Their structures are related to that of their parent dimer, and provide information about any cooperativity that might add to their binding strength.

COMPUTATIONAL DETAILS

The properties of the $(SO_3)_n$:H_2CO complexes (n = 1, 2), were studied through the use of second-order Møller-Plesset perturbation theory (MP2)[50] with the aug-cc-pVDZ basis set.[51, 52] In all cases, vibrational frequencies were calculated in order to confirm that the structures obtained correspond to true minima. All calculations were carried out via the GAUSSIAN09 program (revision D.01).[53] Interaction energies, E_{int}, were computed as the difference in energy between the complex on one hand, and the sum of the energies of the two monomers on the other, using the monomer geometries from the optimized complex. The

binding energy is defined as the difference in energy between the optimized complex and the sum of the two monomers in their optimized geometries. E_{int} was also corrected by the counterpoise procedure with the monomers in their geometry within the complex.[54] In order to obtain more accurate values, single point CCSD(T)[55]/aug-cc-pVTZ calculations were performed for the 1:1 heterodimers.

The many-body procedure[56, 57] was applied to trimers [eqn (1)] whereby the interaction energy can be expressed as:

$$E_{int}\,(\text{trimer}) = \Sigma\Delta^2 E + \Delta^3 E \qquad (1)$$

where $\Delta^n E$ is the n^{th} complex term ($n = 2$ for dimers and 3 for trimers) and the largest value of n represent the total cooperativity in the full complex. Furthermore, E_r, that is, the energy which computes the monomer's deformation, is the link between the interaction (E_{int}) and binding (E_b) energies [eqn (2)], the latter of which is referenced to the fully optimized geometries of the two monomers:

$$E_b = E_{int} + E_r \qquad (2)$$

Atoms in Molecules (AIM)[58, 59] theory at the MP2/aug-cc-pVDZ level, and Natural Bond Orbital (NBO)[60] analysis with the ωB97XD[61] functional and the aug-cc-pVDZ basis set, were applied to analyze the interactions, using the AIMAll[62] and NBO6.0[63] programs. The appearance of an AIM bond critical point (BCP) between centers of different monomers supports the presence of attractive bonding interactions, which can also be examined by NBO charge transfer between orbitals of different fragments.[58, 64]

The molecular electrostatic potential (MEP) on the 0.001 au electron density isosurface at the MP2/aug-cc-pVDZ level was analyzed for the monomers via the WFA-SAS program.[65] Also, for the heterodimers, the electron density shift (EDS) maps were calculated as the difference between the electron density of the complex and the sum of those of the monomers in the geometry of the complex using the GAUSSIAN09 program (revision D.01).[53] Finally, the Localized Molecular Orbital Energy Decomposition Analysis method (LMOEDA)[66] at the MP2/aug-cc-pVDZ computational level was used to decompose the interaction energy terms via eqn (3):

$$E_{int} = E_{elec} + E_{exc} + E_{rep} + E_{pol} + E_{disp} \qquad (3)$$

where E_{elec} is the electrostatic term describing the classical Coulombic interaction between the unperturbed electron densities of the two monomers. E_{exc} and E_{rep} are the exchange and repulsive components associated with the Pauli exclusion principle, and E_{pol} and E_{disp} correspond to polarization and dispersion terms, respectively. The dispersion energy refers to the MP2 correction to the Hartree-Fock interaction energy, which contains mainly dispersion and higher-order corrections to the other terms (electrostatic, exchange, repulsion and polarization). These calculations were carried out with the GAMESS program (version 2013-R1).[67]

RESULTS AND DISCUSSION

Monomers

Sulfur trioxide (SO_3) and formaldehyde (H_2CO) adopt D_{3h} and C_{2v} optimized geometries. Geometries and vibrational frequencies are well described within the MP2/aug-cc-pVDZ level with respect to experimental data: vibrationally averaged structures and anharmonic frequencies[68-71]. [See Table S1 of the electronic supplementary information (ESI)]. For example, a linear correlation is found between the calculated and experimental frequencies ($R^2 = 0.997$) in Table S1.

Their MEPs on the 0.001 au electron density isosurface are displayed in Figure 1, where red and blue colors indicate negative and positive regions, respectively. Two ESP minima (grey dots) are associated with each of the O atoms of SO_3, with values of –8.85 kcal/mol, corresponding to the classical "rabbit ear" lone pair directions. Two local ESP maxima (black dots) are located above and below the central S atom, representing very deep π-holes with values of +52.33 kcal/mol. H_2CO also exhibits two ESP minima associated with the O lone pairs of the carbonyl functional group, but 3-4 times stronger than those of SO_3, with values of –29.18 kcal/mol. There are ESP maxima along the C–H bond extensions, with values of +21.84 kcal/mol, as well as above and below the CH_2 group, with similar values of +24.72 kcal/mol.

SO_3:H_2CO Heterodimers

Exploration of the full potential electrostatic surface (PES) of the SO_3:H_2CO system at the MP2/aug-cc-pVDZ level led to three minima, whose structures are illustrated in Figure 2. There appear to be two strong and short interactions in **A1**. A chalcogen S··O bond with short interatomic distance of 2.414 Å is coupled with a CH··O hydrogen bond (HB) of the same length. CH··O HBs, albeit much longer ones, are contained in **A2**, along with a long and presumably weak O··C interaction (see Figure S1 of the ESI). The same two CH··O HBs involved both H atoms appear in **A3**, but the O··C bond of **A2** is replaced by a third CH··O HB; all three of these HBs are rather long. One can draw immediate correlations between the three minima and the electrostatic potentials of the two monomers: **A1** directly connects the deep π-hole of SO_3

with one of the O lone pair minima of H_2CO; the two H atoms of H_2CO are drawn toward the O_B lone pairs of SO_3 in **A2**; and the O_A lone pair is attracted toward the π-hole of H_2CO. **A3** is stabilized solely by SO_3 O lone pairs and H_2CO H atom attractions.

The interaction energies of the three complexes are reported in Table 1, along with other thermodynamic quantities. It is first evident that **A1** is much more stable than the other two structures, by nearly an order of magnitude. One reason for this distinction can be found in the electrostatic potentials. **A1** combines the deep π-hole of SO_3 with the strong O lone pair minima of H_2CO, while the former π-hole is not involved in **A2** and **A3**. The latter two structures utilize only the O lone pairs of SO_3, which are much weaker than those of H_2CO (–8.85 vs. –29.2 kcal/mol). The entropy, enthalpy, and free energy values for the formation reactions of the three complexes at $T = 298$ K are also displayed in Table 1. The vibrational corrections to ΔE, both zero point and thermal, lead to less negative values of ΔH, in fact making this quantity slightly positive for **A2** and **A3**. Inclusion of the negative entropic factors leads to positive values of ΔG for all three dimers, although **A1** is least positive. Also of note, binding energies are very similar to the interaction energies, a consequence of the very small deformation of the monomer geometries in the complexes (less than 0.04 kcal/mol).

A comparison of SO_3 with SO_2 is of fundamental interest in understanding how the trivalent and divalent molecules differ. An earlier study of the heterodimer of SO_2 with H_2CO found an equilibrium structure very much like **A1** here.[38] The S··O distance was longer by 0.354 Å, but R(O··H) nearly the same. Consistent with the longer R(S··O), the interaction energy of this dimer was 5.42 kcal/mol at the CCSD(T)/aug-cc-pVTZ level, only half that of **A1**. Part of this weaker binding for SO_2 can be traced to its shallower π-hole, 31.25 kcal/mol as compared to 52.33 kcal/mol for SO_3. The stronger π-hole in the latter molecule may in turn be attributed to the presence of a third electron-withdrawing O atom.

As two molecules begin to interact with one another, they perturb one another's electron clouds, and these changes can be monitored via electron density shift (ESD) maps. The maps in Figure 3 were calculated as the difference between the electron density of the complex and the sum of the monomers in the geometry of the complex; purple and green regions indicate, respectively, gains and losses of density that arise due to complexation. Consistent with its shorter intermolecular distance and greater interaction energy, the shifts in **A1** are much larger than in **A2** or **A3**, so much so that a smaller isosurface value was necessary to show the more subtle shifts in the latter two dimers. The CH··O HBs suggested by AIM in Figure 2 and Figure S1 of the ESI are confirmed by the density shifts, which show the expected density loss around the bridging proton and gain in the lone pair region of the proton acceptor O atom, albeit weaker in **A2** and **A3** than in **A1**. With respect to **A1**, the strong S··O chalcogen bond is manifest by green density loss in the region of the S π-hole, and a good deal of purple buildup in the midpoint region

between the S and the O. The AIM concept of an O··C bond in **A2** corresponds to a density increase in the lone pair region of the corresponding SO_3 O atom, and smaller loss in the π region of C.

Another window into the nature of the interaction arises from a dissection of the total interaction energy into its component parts. This decomposition was carried out via the LMOEDA scheme, and the results are presented in Table 2. For all three structures, the repulsion term is the largest in absolute value. Of the various attractive terms, exchange is the most important, followed by electrostatic and polarization for **A1**, and much smaller, dispersion. Exchange is also the largest component in **A2** and **A3**, but dispersion takes second place, followed by electrostatic and polarization.

NBO analysis is particularly adept at identifying particular charge transfers from one molecular orbital to another. The results of such analysis at the ωB97XD/aug-cc-pVDZ level are reported in Table 3. Considering first **A1**, the dominant transfer, amounting to 34.45 kcal/mol, occurs from H_2CO O lone pairs to the S–O_A π* antibonding orbital, consistent with the concept of a S···O chalcogen bond as a primary driving force for complexation. There is also a minor contribution into another SO π* antibond, involving O_C. The $O_{lp}\rightarrow\sigma^*$(CH) transfer is typical of what is expected for a CH··O HB; note the much smaller contribution of this HB as compared to the S···O chalcogen bond. The O··C AIM bond of **A2** corresponds to the $O_{Alp}\rightarrow$ π*(CO) transfer, although the CH··O HBs predicted by AIM for this dimer do not appear in Table 3. While three such CH··O HBs appear in Figure 2 and Figure S1 of the ESI, only one such bond (the shortest) is predicted by NBO.

$(SO_3)_2$:H_2CO Heterotrimers

The PES for the $(SO_3)_2$:H_2CO heterotrimer was explored following a dual strategy: i) the introduction of a second SO_3 monomer to the SO_3:H_2CO minima taking into account their ESP stationary points; and ii) fresh initial structures chosen by random selection[72] were optimized in order to ensure full coverage of the entire PES. The seven most stable minima, which represent essentially the totality of the Boltzmann population are displayed as **B1** to **B7** in Figure 4. All of these geometries are offshoots of the **A1** dimer, with H_2CO and SO_3(1) similarly disposed. With the sole exception of the symmetric **B6** complex (C_{2v}), all trimers have an important characteristic: the S···O bond between SO_3(1) and H_2CO is shorter than it is in **A1** (2.414 Å). See Figure S1 of the ESI. This contraction varies between 0.125 Å in **B1** and 0.081Å in **B7**. In addition to the S··O bond, complexes **B1**-**B4** and **B7** also contain the secondary CH··O_C HB. R(H··O), which is 2.415 Å in dimer **A1**, is also reduced in these complexes, by 0.051 Å (**B4**) to 0.016 Å (**B7**).

With respect to the disposition of the two SO_3 monomers within the ternary complexes, the S of the additional molecule SO_3(2) engages in a S··O bond to SO_3(1) in all seven structures. This interaction is augmented by an O··C bond to the H_2CO in **B1**-**B5**. The latter distance averages 2.862 Å, shorter by 0.244 Å than the O··C distance in the **A2** heterodimer. This contraction indicates enhancement of the

electrophilic character of the C atom due to the presence of SO_3(1) and the S··O bond in which it engages. In several of the dimers, viz. **B2, B4, B5**, and **B7**, the two SO_3 molecules form an O··O chalcogen bond. Symmetric **B6** differs in that both SO_3 monomers are situated as in **A1**. As the central H_2CO acts as double electron donor in two S··O bonds, it is not surprising to note that the R(S··O) distance in **B6** is 0.114 Å longer than in **A1**; likewise for the 0.105 Å longer CH··O HBs. The absence of such O··O bonds in the dimers of Figure 2 is likely due to the Coulombic repulsions between negatively charged regions that surround these atoms. This negative charge is more intense in H_2CO, so its O atom avoids O··O interactions in both dimers and trimers. The weaker negative region around the O atoms of SO_3 permits a certain degree of O··O bonding, albeit weaker, in the trimers. Note for example, that there is no R(O··O) intermolecular distance in Figure 4 that is shorter than 3.2 Å.

Results of a many-body analysis for the most stable $(SO_3)_2$:H_2CO heterotrimers are displayed in Table 4. The three first columns refer to two-body terms, where subscripts 1, 2 and 3 correspond to H_2CO, SO_3 molecule situated as in **A1** [SO_3(1)] and the second SO_3 molecule [SO_3(2)], respectively. It is noteworthy that the quantities obtained for E_{12} in all cases, with the exception of the symmetric **B6** minimum, are more negative than the –11.30 kcal/mol obtained for the interaction energy in **A1**, suggesting that the presence of the second SO_3 molecule enhances the bonding between H_2CO and SO_3(1), consistent with the aforementioned shortened S··O distances. The second SO_3 molecule interacts much less strongly with H_2CO (E_{13}) than does the first, presumably due to the absence of a S··O bond between them (with the obvious exception of **B6**).

The three-body term represents the total cooperativity in the full complex. Negative values of Δ^3E are associated with positive cooperativity; that is, formation of each trimer is energetically favored, while positive values of Δ^3E, represent the opposite.[73] Negative values of Δ^3E may be noted for all trimers with the exception again of **B6**, with values that vary between 1.02 kcal/mol for **B7** up to 2.92 kcal/mol for **B2**.

The total interaction energies vary between –19.10 and –22.06 kcal/mol, categorizing these trimers as very tightly bound. The small differences between the energies of the first few trimers make it difficult to state with certainty which would be most stable at a higher level of theory. On the other hand, MP2/aug-cc-pVTZ//MP2/aug-cc-pVDZ calculations for the three most stable trimers indicate that the order remains intact and the energy differences in fact become larger, with relative energies 0.00, 0.38 and 0.56 kcal/mol, respectively. These results sustain the validity of our methodology. Deformation energies of the monomers needed to conform to the trimer constraints (E_r) are between 0.80 and 2.39 kcal/mol. Adding this deformation energy to the total interaction leads to the binding energies in the last column of Table 4, preserving the energetic ordering of E_{int}.

As in the case of the dimers, NBO analysis complements the type of information derived from AIM. Table 5 reinforces the idea that the strongest binding force arises from the S··O chalcogen bond between SO_3(1) and H_2CO, with $E(2)$ values between 49.83 and 58.29 kcal/mol (for ease of interpretation, all the contributions for a given type of noncovalent bond have been summed: for example, $O_{lp}\rightarrow\pi^*(SO)$ combines $O_{lp}\rightarrow\pi^*(SO_A)$ + $O_{lp}\rightarrow\pi^*(SO_B)$ + $O_{lp}\rightarrow\pi^*(SO_C)$ contributions). Note that this quantity is larger than the same property in the original **A1** dimer, where $E(2)$ was 37.51 kcal/mol, reinforcing the ideas of positive cooperativity arising from geometries and many-body analysis (again, the **B6** trimer is an exception, with its negative cooperativity). The second largest contribution, on the order of 10.35-13.89 kcal/mol, is associated with the interactions between the two SO_3 molecules, typically another S··O chalcogen bond. Much smaller are a range of different tertiary interactions, which include $O_{lp}\rightarrow\sigma^*(CH)$ for CH··O HBs, $\pi(CO)\rightarrow\pi^*(SO)$, and $O_{lp}\rightarrow\pi^*(CO)$.

Relationships between several of the computed properties of the chalcogen bonds in the dimers and trimers were examined, including both those between H_2CO and SO_3, and those between pairs of SO_3 molecules. For instance the electron density at the bond critical point varies exponentially with R(S··O), with $R^2 = 0.997$. Likewise the Laplacian at the same bond critical point varies linearly with R, with $R^2 = 0.981$. The NBO second-order perturbation energy E(2) has an exponential dependence on R with $R^2 = 0.992$, a linear dependence on ρ_{BCP} with $R^2 = 0.998$, and a linear relationship with $\nabla^2\rho_{BCP}$, $R^2 = 0.998$. These functional dependences are consistent with previous reports in the literature.[30, 34, 74]

A simplified means of understanding the cooperativity relies on consideration of how the formation of the dimer affects the electrostatic potential of each monomer. The values of V_{max} and V_{min} in the **A1** dimer are exhibited in Scheme 1, followed by the same quantity in the isolated monomers. For example, the closed circle near the S atom represents the π-hole of SO_3. Formation of the complex with H_2CO reduces V_{max} from 52.33 down to 34.38 kcal/mol, making this S atom a less attractive target for a second S··O chalcogen bond. And indeed, there are no trimers in which a single S atom participates in more than one such S··O bond. In contrast, the π-hole of the C atom experiences an intensification, from 24.72 kcal/mol in H_2CO to 37.44 in the dimer, now competitive with the S π-hole in **A1**. This strong π-hole helps explain the presence of O··C bonds in many of the trimer structures, much shorter than this same bond in the dimer. Also strengthened by dimerization are the σ-holes along the C–H bond extensions of H_2CO, accounting for the shortening of the CH··O HBs in the trimers. V_{min} for the O lone pairs on SO_3 becomes more intense upon pairing with H_2CO. Its value in the monomer is –8.85 kcal/mol, which becomes more negative, to as much as –20.05 kcal/mol in **A1**, another factor in the shortening of the CH··O HBs and the O··C bonds. This sort of profile of enhanced ESP maxima and minima has been used to better understand the sequential inclusion of HCN monomers in homo-oligomers.[73]

CONCLUSIONS

Although there are three minima on the SO_3:H_2CO PES, the global minimum is much more stable than are the other two. This dimer is bound by 10.52 kcal/mol, primarily due to a strong S··O chalcogen bond. The geometry of this dimer places an O lone pair of the H_2CO molecule in close proximity to the positive potential directly above the S atom of SO_3 (a π-hole). There is also a great deal of charge transfer from the former lone pair to the S–O π* antibonding orbital. A smaller contribution arises from a CH··O HB.

When a second SO_3 molecule is added, most of the ensuing heterotrimers contain the structure of the original dimer, and the third molecule placed so that it can interact with both of the original molecules. The latter interactions are varied, but the strongest of these include a S··O chalcogen bond between SO_3 molecules, an O··C bond, O··O chalcogen bond, and a CH··O HB. These trimers are tightly bound, with total interaction energies as high as 22.06 kcal/mol. Many of the trimer structures show positive cooperativity, with shortened S··O distances, and three-body interaction energies of nearly 3 kcal/mol.

SUPPLEMENTARY MATERIAL

Electronic supplementary information (ESI) available. See DOI: 10.1039/c3cpXXXXXX

ACKNOWLEDGMENTS

This work has been supported by NSF-CHE-1026826 and CTQ2012-35513-C02-02 (MINECO) Projects. Also, LMA thanks the MICINN for a PhD grant (No. BES-2010-031225). Computer, storage and other resources from the Division of Research Computing in the Office of Research and Graduate Studies at Utah State University and the CTI (CSIC) are gratefully acknowledged.

REFERENCES

1. P. Hobza and K. Müller-Dethlefs, *Non-Covalent Interactions*, The Royal Society of Chemistry, Cambridge, UK, 2009.
2. P. Schuster, G. Zundel and C. Sandorfy, *The Hydrogen Bond. Recent Developments in Theory and Experiments*, North-Holland Publishing Co., Amsterdam, The Netherlands, 1976.
3. S. Scheiner, *Hydrogen Bonding: A Theoretical Perspective*, Oxford University Press, New York, USA, 1997.
4. S. J. Grabowski, *Hydrogen Bonding - New Insights*, Springer, Dordrecht, The Netherlands, 2006.
5. G. Gilli and P. Gilli, *The Nature of the Hydrogen Bond*, Oxford University Press, Oxford, UK, 2009.
6. J. P. M. Lommerse, A. J. Stone, R. Taylor and F. H. Allen, *J. Am. Chem. Soc.*, 1996, **118**, 3108-3116.
7. P. Metrangolo and G. Resnati, *Science*, 2008, **321**, 918-919.
8. W. Zierkiewicz, D. Michalska and T. Zeegers-Huyskens, *Phys. Chem. Chem. Phys.*, 2010, **12**, 13681-13691.
9. U. Adhikari and S. Scheiner, *Chem. Phys. Lett.*, 2012, **532**, 31-35.
10. P. Politzer, J. S. Murray and T. Clark, *Phys. Chem. Chem. Phys.*, 2013, **15**, 11178-11189.
11. M. Solimannejad, M. Malekani and I. Alkorta, *J. Phys. Chem. A*, 2013, **117**, 5551-5557.
12. S. Tschirschwitz, P. Lonnecke and E. Hey-Hawkins, *Dalton Trans.*, 2007, DOI: 10.1039/b617257a, 1377-1382.
13. M. Bühl, P. Kilian and J. D. Woollins, *ChemPhysChem*, 2011, **12**, 2405-2408.
14. J. E. Del Bene, I. Alkorta, G. Sanchez-Sanz and J. Elguero, *Chem. Phys. Lett.*, 2011, **512**, 184-187.
15. S. Scheiner, *J. Phys. Chem. A*, 2011, **115**, 11202-11209.
16. S. Zahn, R. Frank, E. Hey-Hawkins and B. Kirchner, *Chem. Eur. J.*, 2011, **17**, 6034-6038.
17. U. Adhikari and S. Scheiner, *Chem. Phys. Lett.*, 2012, **536**, 30-33.
18. S. Scheiner, *Acc. Chem. Res.*, 2012, **46**, 280-288.
19. I. Alkorta, J. Elguero and J. E. Del Bene, *J. Phys. Chem. A*, 2013, **117**, 4981-4987.
20. L. M. Azofra, I. Alkorta and J. Elguero, *ChemPhysChem*, 2014, **in press**, DOI: 10.1002/cphc.201402086.
21. I. Alkorta, I. Rozas and J. Elguero, *J. Phys. Chem. A*, 2001, **105**, 743-749.
22. L. M. Azofra, M. Altarsha, M. F. Ruiz-López and F. Ingrosso, *Theor. Chem. Acc.*, 2013, **132**, 1326.
23. A. Bauzá, T. J. Mooibroek and A. Frontera, *Angew. Chem. Int. Ed.*, 2013, **52**, 12317-12321.
24. S. J. Grabowski, *Phys. Chem. Chem. Phys.*, 2014, **16**, 1824-1834.
25. R. E. Rosenfield, R. Parthasarathy and J. D. Dunitz, *J. Am. Chem. Soc.*, 1977, **99**, 4860-4862.
26. F. T. Burling and B. M. Goldstein, *J. Am. Chem. Soc.*, 1992, **114**, 2313-2320.
27. M. Iwaoka, S. Takemoto and S. Tomoda, *J. Am. Chem. Soc.*, 2002, **124**, 10613-10620.
28. D. B. Werz, R. Gleiter and F. Rominger, *J. Am. Chem. Soc.*, 2002, **124**, 10638-10639.
29. C. Bleiholder, D. B. Werz, H. Köppel and R. Gleiter, *J. Am. Chem. Soc.*, 2006, **128**, 2666-2674.
30. G. Sánchez-Sanz, I. Alkorta and J. Elguero, *Mol. Phys.*, 2011, **109**, 2543-2552.
31. M. Jabłoński, *J. Phys. Chem. A*, 2012, **116**, 3753-3764.
32. G. Sánchez-Sanz, C. Trujillo, I. Alkorta and J. Elguero, *ChemPhysChem*, 2012, **13**, 496-503.
33. U. Adhikari and S. Scheiner, *J. Phys. Chem. A*, 2014, **118**, 3183-3192.
34. L. M. Azofra and S. Scheiner, *J. Phys. Chem. A*, 2014, **118**, 3835-3845.
35. L. M. Azofra, I. Alkorta and S. Scheiner, *J. Chem. Phys.*, 2014, **140**, 244311.
36. J. T. Goettel, P. Chaudhary, P. Hazendonk, H. P. A. Mercier and M. Gerken, *Chem. Commun.*, 2012, **48**, 9120-9122.
37. J. Murray, P. Lane, T. Clark, K. Riley and P. Politzer, *J. Mol. Model.*, 2012, **18**, 541-548.

38. L. M. Azofra and S. Scheiner, *J. Chem. Phys.*, 2014, **140**, 034302.
39. L. M. Azofra and S. Scheiner, *Phys. Chem. Chem. Phys.*, 2014, **16**, 5142-5149.
40. J. S. Murray, P. Lane and P. Politzer, *Int. J. Quantum Chem.*, 2007, **107**, 2286-2292.
41. P. Politzer, J. Murray and M. Concha, *J. Mol. Model.*, 2008, **14**, 659-665.
42. J. Murray, P. Lane and P. Politzer, *J. Mol. Model.*, 2009, **15**, 723-729.
43. O. B. Gadzhiev, S. K. Ignatov, M. Y. Kulikov, A. M. Feigin, A. G. Razuvaev, P. G. Sennikov and O. Schrems, *J. Chem. Theory Comput.*, 2012, **9**, 247-262.
44. G. E. Likens and F. H. Bormann, *Science*, 1974, **184**, 1176-1179.
45. J. G. Calvert, A. Lazrus, G. L. Kok, B. G. Heikes, J. G. Walega, J. Lind and C. A. Cantrell, *Nature*, 1985, **317**, 27-35.
46. J. P. D. Abbatt and M. J. Molina, *Annu. Rev. Energy Env.*, 1993, **18**, 1-29.
47. S. Solomon, *Rev. Geophys.*, 1999, **37**, 275-316.
48. M. Norval, R. M. Lucas, A. P. Cullen, F. R. de Gruijl, J. Longstreth, Y. Takizawa and J. C. van der Leun, *Photochem. Photobiol. Sci.*, 2011, **10**, 199-225.
49. M. C. Cooke, S. R. Utembe, P. G. Carbajo, A. T. Archibald, A. J. Orr-Ewing, M. E. Jenkin, R. G. Derwent, D. J. Lary and D. E. Shallcross, *Atmos. Sci. Let.*, 2010, **11**, 33-38.
50. C. Møller and M. S. Plesset, *Phys. Rev.*, 1934, **46**, 618-622.
51. T. H. J. Dunning, *J. Chem. Phys.*, 1989, **90**, 1007-1023.
52. D. E. Woon and T. H. Dunning, *J. Chem. Phys.*, 1993, **98**, 1358-1371.
53. M. J. Frisch, G. W. Trucks, H. B. Schlegel, G. E. Scuseria, M. A. Robb, J. R. Cheeseman, G. Scalmani, V. Barone, B. Mennucci, G. A. Petersson, H. Nakatsuji, M. Caricato, X. Li, H. P. Hratchian, A. F. Izmaylov, J. Bloino, G. Zheng, J. L. Sonnenberg, M. Hada, M. Ehara, K. Toyota, R. Fukuda, J. Hasegawa, M. Ishida, T. Nakajima, Y. Honda, O. Kitao, H. Nakai, T. Vreven, J. Montgomery, J. A., J. E. Peralta, F. Ogliaro, M. Bearpark, J. J. Heyd, E. Brothers, K. N. Kudin, V. N. Staroverov, R. Kobayashi, J. Normand, K. Raghavachari, A. Rendell, J. C. Burant, S. S. Iyengar, J. Tomasi, M. Cossi, N. Rega, N. J. Millam, M. Klene, J. E. Knox, J. B. Cross, V. Bakken, C. Adamo, J. Jaramillo, R. Gomperts, R. E. Stratmann, O. Yazyev, A. J. Austin, R. Cammi, C. Pomelli, J. W. Ochterski, R. L. Martin, K. Morokuma, V. G. Zakrzewski, G. A. Voth, P. Salvador, J. J. Dannenberg, S. Dapprich, A. D. Daniels, Ö. Farkas, J. B. Foresman, J. V. Ortiz, J. Cioslowski and D. J. Fox, GAUSSIAN09, Revision D.01, Wallingford CT, 2009.
54. S. F. Boys and F. Bernardi, *Mol. Phys.*, 1970, **19**, 553-566.
55. J. A. Pople, M. Head-Gordon and K. Raghavachari, *J. Chem. Phys.*, 1987, **87**, 5968-5975.
56. S. S. Xantheas and T. H. Dunning, *J. Chem. Phys.*, 1993, **99**, 8774-8792.
57. S. S. Xantheas, *J. Chem. Phys.*, 1994, **100**, 7523-7534.
58. R. F. W. Bader, *Atoms in Molecules: A Quantum Theory*, Clarendon Press, Oxford, UK, 1990.
59. P. L. A. Popelier, *Atoms In Molecules. An introduction*, Prentice Hall, Harlow, UK, 2000.
60. F. Weinhold and C. R. Landis, *Valency and Bonding. A Natural Bond Orbital Donor-Aceptor Perspective*, Cambridge Press, Cambridge, UK, 2005.
61. J.-D. Chai and M. Head-Gordon, *Phys. Chem. Chem. Phys.*, 2008, **10**, 6615-6620.
62. T. A. Keith, AIMAll (Version 13.11.04), Overland Park KS, USA, 2013.
63. E. D. Glendening, J. K. Badenhoop, A. E. Reed, J. E. Carpenter, J. A. Bohmann, C. M. Morales, C. R. Landis and F. Weinhold, NBO 6.0, Madison, USA, 2013.
64. I. Rozas, I. Alkorta and J. Elguero, *J. Am. Chem. Soc.*, 2000, **122**, 11154-11161.
65. F. Bulat, A. Toro-Labbé, T. Brinck, J. Murray and P. Politzer, *J. Mol. Model.*, 2010, **16**, 1679-1691.
66. P. Su and H. Li, *J. Chem. Phys.*, 2009, **131**, 014102.
67. M. W. Schmidt, K. K. Baldridge, J. A. Boatz, S. T. Elbert, M. S. Gordon, J. H. Jensen, S. Koseki, N. Matsunaga, K. A. Nguyen, S. Su, T. L. Windus, M. Dupuis and J. A. Montgomery, *J. Comput. Chem.*, 1993, **14**, 1347-1363.

68. T. Shimanouchi, H. Matsuura, Y. Ogawa and I. Harada, *J. Phys. Chem. Ref. Data*, 1978, **7**, 1323-1444.
69. T. Nakanaga, S. Kondo and S. Saëki, *J. Chem. Phys.*, 1982, **76**, 3860-3865.
70. L. V. Gurvich, *Pure Appl. Chem.*, 1989, **61**, 1027-1031.
71. V. Meyer, D. Hermann Sutter and H. Dreizler, *Z. Naturforsch. A Phys. Sci.*, 1991, **46**, 710-714.
72. A. P. Sergeeva, B. B. Averkiev, H.-J. Zhai, A. I. Boldyrev and L.-S. Wang, *J. Chem. Phys.*, 2011, **134**, 224304.
73. I. Alkorta, F. Blanco, P. Deyà, J. Elguero, C. Estarellas, A. Frontera and D. Quiñonero, *Theor. Chem. Acc.*, 2010, **126**, 1-14.
74. U. Koch and P. L. A. Popelier, *J. Phys. Chem.*, 1995, **99**, 9747-9754.

Table 1. Binding, E_b, and interaction, E_{int}, energies for the SO_3:H_2CO heterodimers at MP2/aug-cc-pVDZ and E_{int} at CCSD(T)/aug-cc-pVTZ//MP2/aug-cc-pVDZ computational levels. Also, entropy, enthalpy and Gibbs free energy for the association reactions at room temperature (298 K) at MP2/aug-cc-pVDZ computational level. All quantities in kcal/mol, except ΔS, in cal K^{-1} mol^{-1}.

	MP2					CCSD(T)[a]
Dimer	E_b	E_{int}[b]	ΔS	ΔH[c]	ΔG[c]	E_{int}[b]
A1	–11.34	–11.30 (–8.57)	–30.49	–5.92	3.17	–11.70 (–10.52)
A2	–1.85	–1.87 (–0.90)	–15.72	0.33	5.02	–1.56 (–1.06)
A3	–1.72	–1.73 (–0.85)	–13.42	0.38	4.38	–1.57 (–1.11)

[a]CCSD(T)/aug-cc-pVTZ//MP2/aug-cc-pVDZ computational level.

[b]Counterpoise corrections to basis set superposition error (BSSE) added in parentheses.

[c]Counterpoise corrections included.

Table 2. LMOEDA energy components, in kcal/mol, for the SO_3:H_2CO heterodimers calculated at the MP2/aug-cc-pVDZ level.

Complex	E_{elec}	E_{exc}	E_{rep}	E_{pol}	E_{disp}	E_{int}
A1	–21.88	–27.37	52.75	–13.46	–1.80	–11.76
A2	–0.86	–2.93	4.89	–0.70	–2.27	–1.87
A3	–1.05	–2.26	3.80	–0.59	–1.63	–1.73

Table 3. Second-order perturbation NBO energy, $E(2)$, in kcal/mol, for the SO_3:H_2CO heterodimers at ωB97XD/aug-cc-pVDZ computational level, above threshold of 0.5 kcal/mol.

Complex	Donor/Acceptor	Type	$E(2)$
A1	H_2CO/SO_3	$O_{lp}\rightarrow\pi^*(SO_A)$	34.45
	H_2CO/SO_3	$O_{lp}\rightarrow\pi^*(SO_B)$	2.07
	H_2CO/SO_3	$O_{lp}\rightarrow\pi^*(SO_C)$	0.99
	SO_3/H_2CO	$O_{Clp}\rightarrow\sigma^*(CH)$	1.52
A2	SO_3/H_2CO	$O_{Alp}\rightarrow\pi^*(CO)$	0.84
A3	SO_3/H_2CO	$O_{Alp}\rightarrow\sigma^*(CH)$	0.68

Table 4. Many-body analysis, in kcal/mol, for the most stable $(SO_3)_2$:H_2CO heterotrimers calculated at MP2/aug-cc-pVDZ computational level. Subscripts 1, 2 and 3 refer to H_2CO, SO_3 molecule from **A1** [$SO_3(1)$], and the second SO_3 molecule [$SO_3(2)$], respectively.

Comp.	E_{12}	E_{13}	E_{23}	$\Sigma\Delta^2E$	Δ^3E	E_{int}	E_r	E_b
B1	–11.82	–2.15	–5.34	–19.31	–2.75	–22.06	2.39	–19.67
B2	–11.60	–2.40	–4.92	–18.92	–2.92	–21.84	2.38	–19.46
B3	–11.94	–1.69	–5.38	–19.01	–2.69	–21.70	2.31	–19.39
B4	–11.82	–2.61	–4.82	–19.25	–2.40	–21.65	2.27	–19.38
B5	–11.54	–2.17	–4.92	–18.63	–2.60	–21.23	2.23	–19.00
B6	–10.52	–10.52	–0.05	–21.09	1.67	–19.42	0.80	–18.62
B7	–11.64	–1.13	–5.31	–18.08	–1.02	–19.10	1.69	–17.41

Table 5. Condensed[a] second-order perturbation NBO energy, $E(2)$, in kcal/mol, for the $(SO_3)_2$:H_2CO heterotrimers at ωB97XD/aug-cc-pVDZ computational level.

Complex	Donor/Acceptor	Type	$E(2)$
B1	$H_2CO/SO_3(1)$	$O_{lp}\rightarrow\pi^*(SO)$	58.29
	$H_2CO/SO_3(1)$	$\pi(CO)\rightarrow\pi^*(SO)$	0.63
	$SO_3(1)/H_2CO$	$O_{lp}\rightarrow\sigma^*(CH)$	1.69
	$SO_3(2)/H_2CO$	$O_{lp}\rightarrow\pi^*(CO)$	0.50
	$SO_3(1)/SO_3(2)$	$O_{lp}\rightarrow\pi^*(SO)$	13.89
B2	$H_2CO/SO_3(1)$	$O_{lp}\rightarrow\pi^*(SO)$	57.02
	$H_2CO/SO_3(1)$	$\pi(CO)\rightarrow\pi^*(SO)$	0.81
	$SO_3(1)/H_2CO$	$O_{lp}\rightarrow\sigma^*(CH)$	0.78
	$SO_3(2)/H_2CO$	$O_{lp}\rightarrow\pi^*(CO)$	1.39
	$SO_3(1)/SO_3(2)$	$O_{lp}\rightarrow\pi^*(SO)$	13.64
B3	$H_2CO/SO_3(1)$	$O_{lp}\rightarrow\pi^*(SO)$	54.33
	$SO_3(1)/H_2CO$	$O_{lp}\rightarrow\sigma^*(CH)$	1.04
	$SO_3(2)/H_2CO$	$O_{lp}\rightarrow\pi^*(CO)$	0.73
	$SO_3(1)/SO_3(2)$	$O_{lp}\rightarrow\pi^*(SO)$	13.17
B4	$H_2CO/SO_3(1)$	$O_{lp}\rightarrow\pi^*(SO)$	56.38
	$H_2CO/SO_3(1)$	$\pi(CO)\rightarrow\pi^*(SO)$	0.56
	$SO_3(1)/H_2CO$	$O_{lp}\rightarrow\sigma^*(CH)$	1.73
	$SO_3(2)/H_2CO$	$O_{lp}\rightarrow\pi^*(CO)$	1.04
	$SO_3(1)/SO_3(2)$	$O_{lp}\rightarrow\pi^*(SO)$	12.15
B5	$H_2CO/SO_3(1)$	$O_{lp}\rightarrow\pi^*(SO)$	53.95
	$H_2CO/SO_3(1)$	$\pi(CO)\rightarrow\pi^*(SO)$	0.52
	$SO_3(1)/H_2CO$	$\pi(SO)\rightarrow\pi^*(CO)$	0.52
	$SO_3(2)/H_2CO$	$O_{lp}\rightarrow\pi^*(CO)$	3.28
	$SO_3(1)/SO_3(2)$	$O_{lp}\rightarrow\pi^*(SO)$	12.38
B6	H_2CO/SO_3	$O_{lp}\rightarrow\pi^*(SO)$	18.88[b]
	SO_3/H_2CO	$O_{lp}\rightarrow\sigma^*(CH)$	1.54[b]
B7	$H_2CO/SO_3(1)$	$O_{lp}\rightarrow\pi^*(SO)$	49.83

$SO_3(1)/H_2CO$	$O_{lp}\rightarrow\sigma^*(CH)$	1.08
$SO_3(1)/SO_3(2)$	$O_{lp}\rightarrow\pi^*(SO)$	10.35

[a]Sum of all the contributions for a given type of noncovalent bond. For example, $O_{lp}\rightarrow\pi^*(SO)$ may refer to $O_{lp}\rightarrow\pi^*(SO_A)$ + $O_{lp}\rightarrow\pi^*(SO_B)$ + $O_{lp}\rightarrow\pi^*(SO_C)$ contributions.

[b]Due to the C_{2v} symmetry, contributions are equal for $SO_3(1)$ and $SO_3(2)$.

Figure 1. Molecular electrostatic potential (MEP) on the 0.001 au electron density isosurface for the isolated SO_3 and H_2CO monomers, both calculated at the MP2/aug-cc-pVDZ computational level. The red and blue colors indicate negative and positive regions, respectively, varying between –0.015 and +0.055 au for SO_3, and between –0.040 and +0.050 au for H_2CO. Black and grey dots indicate the location of the ESP maxima and minima, respectively, on the surface. Frontal and lateral views are shown for each.

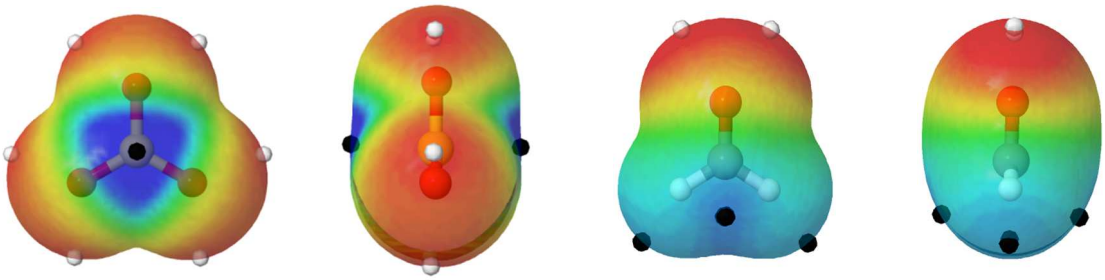

SO_3 (D_{3h}) H_2CO (C_{2v})

Figure 2. Structures of the SO_3:H_2CO heterodimers optimized at the MP2/aug-cc-pVDZ computational level. Broken blue lines link atoms which present interatomic AIM BCPs, with interatomic distances in Å. (See Figure S1 of the ESI for more complete analysis.) Complexes are arranged in ascending order of energy.

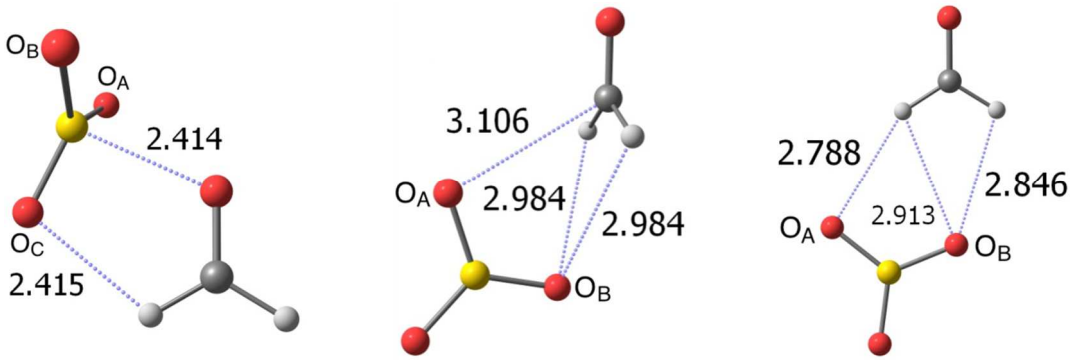

A1 (C_s) **A2** (C_s) **A3** (C_1)

Figure 3. Electron density shifts (EDS) for the SO_3:H_2CO heterodimers calculated at the MP2/aug-cc-pVDZ level. Purple and green refer to gain and loss of density, respectively, relative to isolated monomers. The values of the isosurfaces are ±0.002 au for **A1**, and ±0.0002 au for **A2** and **A3**.

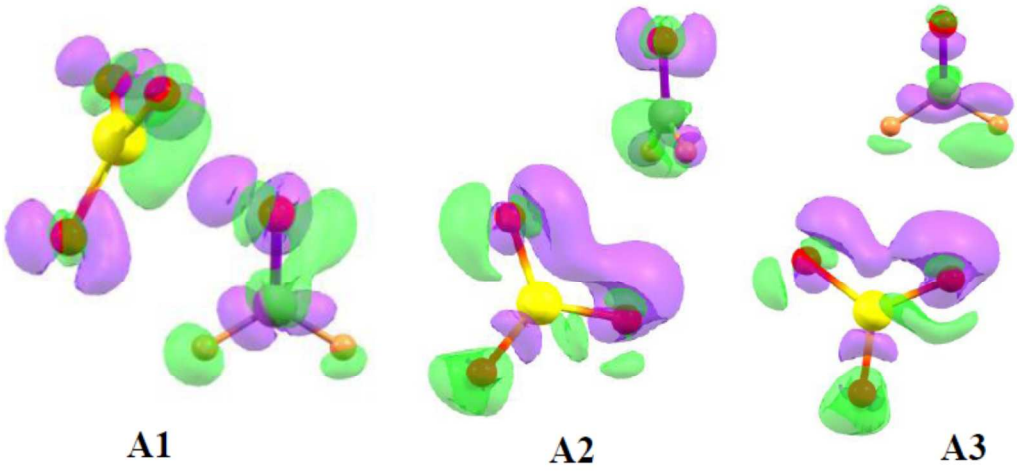

Figure 4. Most stable structures of the $(SO_3)_2$:H_2CO PES optimized at the MP2/aug-cc-pVDZ computational level. Broken lines link atoms which present interatomic AIM BCPs, with interatomic distances in Å. (See Figure S1 of the ESI for more complete analysis.) Complexes are arranged in ascending order of energy. Index (1) refers to the SO_3 monomer situated as in dimer **A1**.

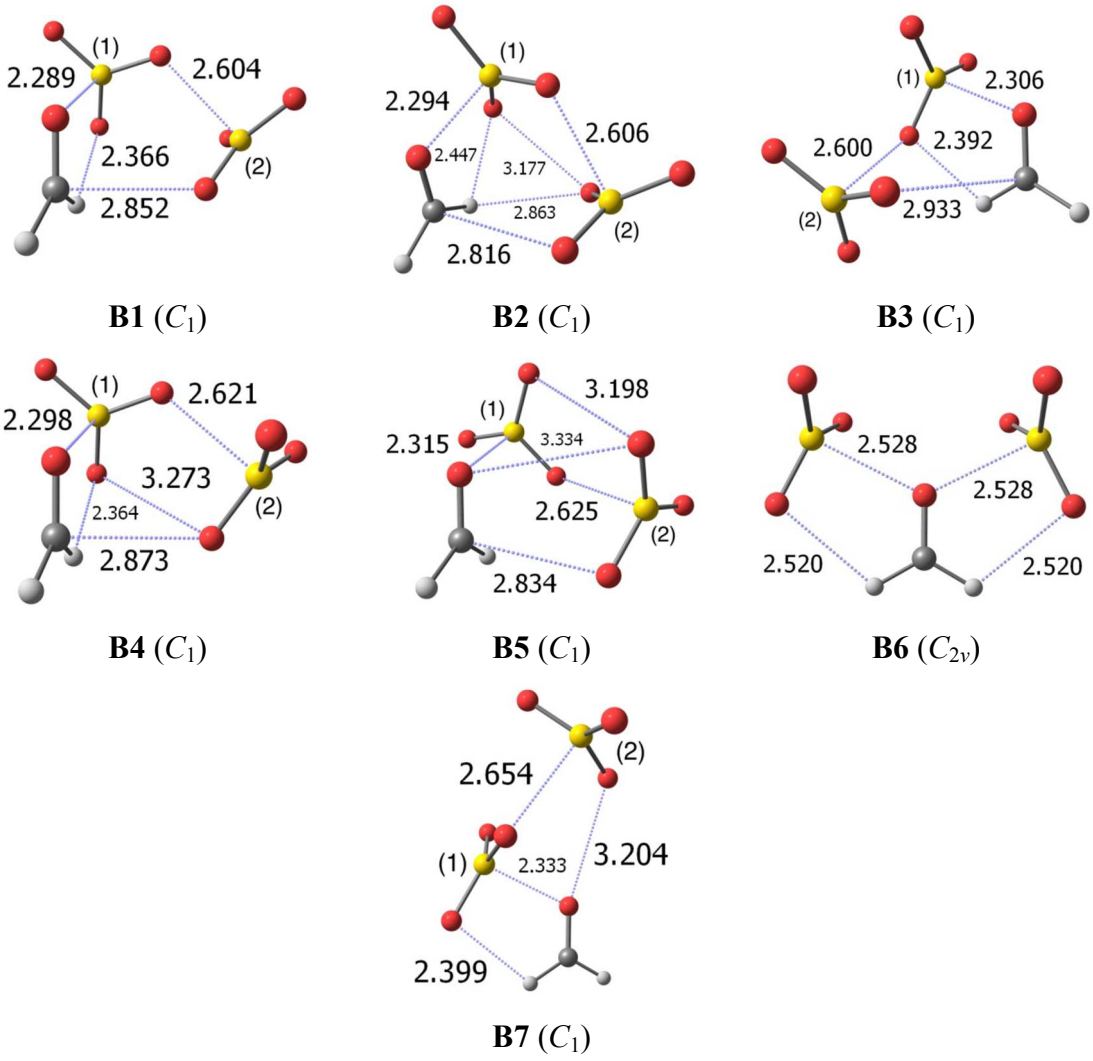

B1 (C_1) **B2** (C_1) **B3** (C_1)

B4 (C_1) **B5** (C_1) **B6** (C_{2v})

B7 (C_1)

Scheme 1. ESP maxima (filled circles) and minima (open circles) in the **A1** SO_3:H_2CO heterodimer. Numerical values, in kcal/mol, refer to V_{max} or V_{min} in the dimer, followed by the same quantity in the isolated monomers (in italics).

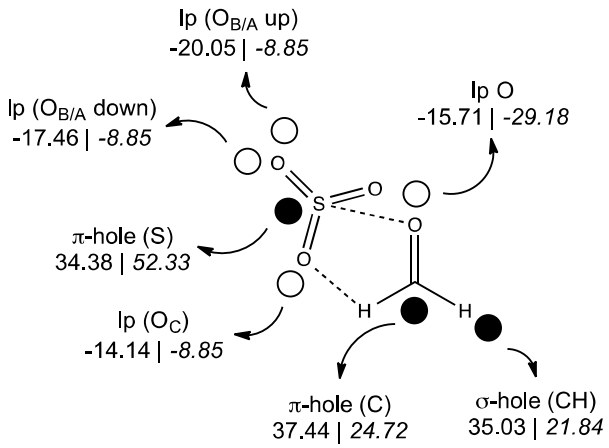

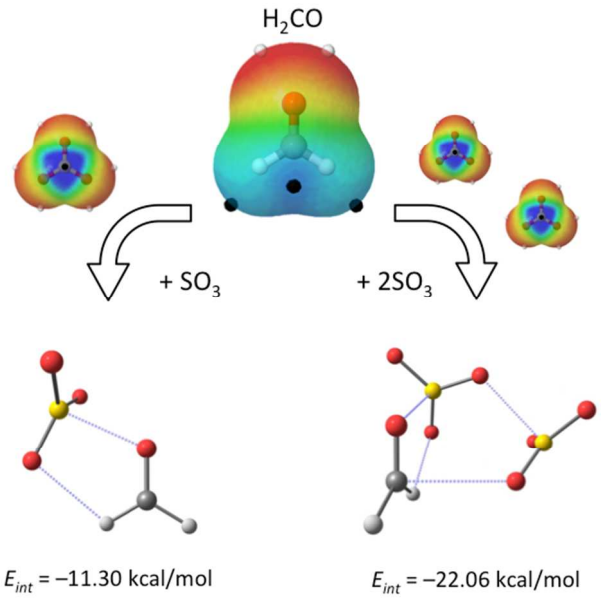

SO_3 and H_2CO dimers and trimers are held together by S··O chalcogen bonds, supplemented by weaker CH··O or O··C bonds.